applied optics

D-shaped photonic crystal fiber plasmonic refractive index sensor based on gold grating

Junjie Lu,[1] Yan Li,[1,*] Yanhua Han,[1] Yi Liu,[1] and Jianmin Gao[2]

[1]Department of Optoelectronics Science, Harbin Institute of Technology, Weihai 264209, China
[2]School of Energy Science and Engineering, Harbin Institute of Technology, Harbin 150001, China
*Corresponding author: liy@hit.edu.cn

Received 23 March 2018; revised 21 May 2018; accepted 24 May 2018; posted 30 May 2018 (Doc. ID 326776); published 25 June 2018

In this work, we proposed a high-resolution D-shaped photonic crystal fiber (PCF) surface plasmon resonance (SPR) sensor based on gold grating. Gold grating is introduced to modulate the resonance wavelength and enhance the refractive index (RI) sensitivity. Structure parameters of PCF and gold grating are analyzed by the finite element method for optimizing the SPR sensor. The simulation results indicate that air hole pitch, air hole diameter, and gold thickness and grating constant have little influence on the sensitivity of the refractive index, which reduces the requirement of precise processing. For improving the resolution of RI sensing, a two-feature (2F) interrogation method, which combines wavelength interrogation and amplitude interrogation, is used. The maximum theoretical resolution of the SPR sensor reaches to 5.98×10^{-6} RIU in the range of 1.36–1.38, and the wavelength sensitivity reaches to 3340 nm/RIU. The proposed SPR sensor shows potential applications for developing a high-sensitivity, real-time, and fast-response SPR-RI sensor.

OCIS codes: (060.2370) Fiber optics sensors; (240.6680) Surface plasmons; (060.5295) Photonic crystal fibers; (280.4788) Optical sensing and sensors.

https://doi.org/10.1364/AO.57.005268

1. INTRODUCTION

Surface plasmon resonance (SPR) is considered a promising method to detect tiny refractive index (RI) changes because SPR is extremely sensitive to permittivity of the surrounding environment. During the past decade, high sensitivity and real-time detection have made the SPR sensor widely used in chemical and biological sensing [1,2]. In recent years, an SPR sensor based on photonic crystal fiber (PCF) has attracted a lot of attention since the first SPR sensor was proposed by Jorgenson in 1993, where the fiber core was coated with gold film by removing a section of the fiber cladding to exhibit the plasmonic response [3]. PCF brings new vitality to the fabrication of SPR sensors due to its unique ability of controlling the evanescent wave penetration. When a phase-matching condition is met, the surface plasmon polaritons (SPP) mode can be excited and result in strong resonance absorption. By detecting the resonance wavelength, unknown analyte RI can be calculated. For investigating the performance of an SPR sensor, many PCF structures, such as dual-core PCF [4], D-shaped PCF [5,6], and birefringent PCF [7] have been well studied in the last decade. For improving the performance of the PCF-SPR sensors, some theoretical designs of metal-coated large air hole PCF-SPR sensors have been reported [8,9]. For instance, Hassani and Skorobogatiy designed a PCF with large air holes; further, they coated the inner surfaces of the air holes with metal films to fabricate the PCF-SPR sensor in which the large air holes were used as micro-channels. The simulation results showed that the resolution of their sensor could reach 10^{-4} RIU [10]. For realizing extremely high sensitivity, larger diameter air holes and a multichannel analyte-filled PCF structure are proposed. Fan *et al.* presented a high-sensitivity RI sensor based on two large air hole channels filled with analyte in which wavelength sensitivity reaches to 7040 nm/RIU [11]. Most of the reported PCF SPR sensors are coated with the multiple metal layer, and liquid is filled inside the air holes for increasing the sensitivity, which is difficult in terms of fabrication. Moreover, because the metal film is coated inside the air holes, it is difficult to precisely control the thicknesses of the metal film, and it is also time-consuming to fill and re-fill the analyte from the air holes.

In this paper, we proposed a SPR sensor based on D-shaped PCF, which is coated with gold grating for improving the RI sensitivity. Gold grating results in more loss of core mode, and, by changing the grating constant, the resonance wavelength could be modulated. The resonance wavelength is sensitive to the surrounding refractive index of gold grating, which shows promising potential in RI sensing. Simulation results show that the RI sensitivity is four times as much as a normal D-shaped PCF-SPR sensor with gold film. By investigating the structure parameters of PCF, simulation results show that PCF

structure has little influence on the sensitivity of SPR sensor. Furthermore, the two-feature (2F) interrogation method is used to provide a higher resolution for RI sensing. In the RI range of 1.36–1.38, the wavelength sensitivity reaches to 3340 nm/RIU, and the maximum theoretical resolution reaches to 5.98×10^{-6} RIU, which is much higher than those of wavelength and intensity interrogation method.

2. DESIGN AND ANALYSIS

The proposed PCF-SPR sensor is shown in Fig. 1(a). There are two type air holes in the PCF, which is side polished with 3 μm depth for creating a plane sensing area. Before fabricating the gold grating, gold film should be coated on the plane surface of D-shaped PCF by magnetron sputtering or pulsed laser deposition. Then, a gold grating can be fabricated by using electron-beam lithography or photolithography. The cross section of the SPR sensor is shown in Fig. 1(b). The diameter of small air holes is $d_s = 0.8$ μm, and the diameter of large air holes is $d_l = 1.6$ μm, respectively. The lattice pitch between all air holes is $\Lambda = 2.3$ μm. The thickness of the gold gratings is $h_g = 40$ nm. The gold grating constant is $d_0 = 1$ μm and duty ratio is $\eta = 0.5$.

The used fiber material is fused silica, and the RI is determined by Sellmeier equation [12] as

$$n(\lambda) = \sqrt{1 + \frac{A_1\lambda^2}{\lambda^2 - B_1} + \frac{A_2\lambda^2}{\lambda^2 - B_2} + \frac{A_3\lambda^2}{\lambda^2 - B_3}}, \quad (1)$$

where $A_1 = 0.696166300$, $A_2 = 0.407942600$, $A_3 = 0.897479400$, $B_1 = 4.67914826 \times 10^{-3}$ μm^2, $B_2 = 1.35120631 \times 10^{-2}$ μm^2, and $B_3 = 97.9340025$ μm^2. The complex dielectric constant of gold is given by Johnson and Christy [13]. The confinement loss is calculated by using the imaginary part of the effective RI:

$$\alpha = 8.686 \times k_0 \times \mathrm{Im}(n_{\mathrm{eff}}) \times 10^4 \ \mathrm{dB/cm}, \quad (2)$$

where $k_0 = 2\pi/\lambda$ is the wavenumber and $\mathrm{Im}(n_{\mathrm{eff}})$ is the imaginary part of effective index. The Gaussian beam propagates along the z-direction and mode analysis is performed in the $X - Y$ plane.

We investigated the sensitivity difference between SPR sensor with gold film and gold grating. As shown in Fig. 2(a), when the thickness of gold is 40 nm and the RI of analyte changes from 1.36 to 1.37, the resonance wavelength of SPR sensor with full coated gold film shifts from 1389.40 to 1397.14 nm, which means the wavelength sensitivity is 774 nm/RIU, which

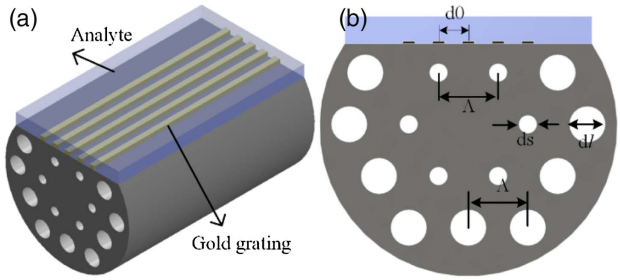

Fig. 1. Schematic of proposed PCF-SPR sensor: (a) 3D view; (b) cross-section of sensor.

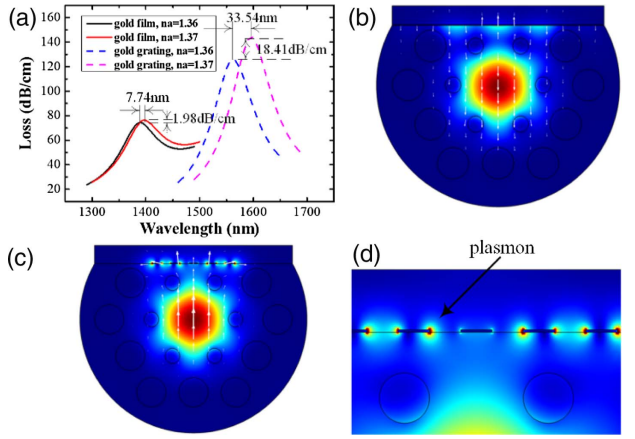

Fig. 2. (a) Resonance wavelength of gold film SPR sensor and gold grating SPR sensor with RI from 1.36 to 1.37. (b) The electric field of full coated gold film SPR sensor. (c) The electric field of gold grating SPR sensor. (d) Intensity distribution of SPP mode.

is not ideal for RI sensing. The electric field of a full coated gold film SPR sensor is shown in Fig. 2(b). Because the wavelength of a common commercial broadband laser source is less than 2 μm, resonance peaks of more than 2 μm are abandoned. However, when the gold film is replaced with gold grating, which could be fabricated by laser direct writing or photolithography, the resonance wavelength shifts significantly, as shown in Fig. 2(a). The wavelength difference is 33.54 nm, as the resonance wavelength shifts from 1562.56 to 1596.10 nm, which means the wavelength sensitivity is 3354 nm/RIU. The simulation result shows that, by introducing the gold grating, the wavelength sensitivity of the SPR sensor is four times that of a normal gold film SPR sensor. Moreover, the amplitude sensitivity of a gold film SPR sensor is –2.66 RIU^{-1}, and the gold grating SPR sensor is –14.61 RIU^{-1}. The gold grating can enhance the loss of the core mode, which results in high amplitude sensitivity.

The electric field of the gold grating SPR sensor is shown in Fig. 2(c), in which the resonance wavelength is 1562.56 nm. Besides the y-polarized core mode, we also can see that the SPP mode appears on the interface of the gold grating and dielectric, as shown in Fig. 2(d). There is strong coupling between the core mode and SPP mode, when the resonance wavelength is 1562.56 nm. Therefore, strong coupling results in high confinement loss and high amplitude sensitivity.

3. RESULTS AND DISCUSSION

Considering the practical fabrication of the PCF, the diameter of air holes is investigated. The confinement loss spectra are shown in Fig. 3(a), when the diameter of small holes (d_s) changes from 0.7 μm to 0.9 μm, and the maximum loss changes from 149.83 dB/cm to 173.48 dB/cm. The wavelength sensitivity could be calculated as [14]

$$Sw = \frac{\Delta\lambda_{\mathrm{peak}}}{\Delta n_a}, \quad (3)$$

where $\Delta\lambda_{\mathrm{peak}}$ is the difference between the two resonance wavelengths, and Δn_a is the variation of analyte RI. As shown in

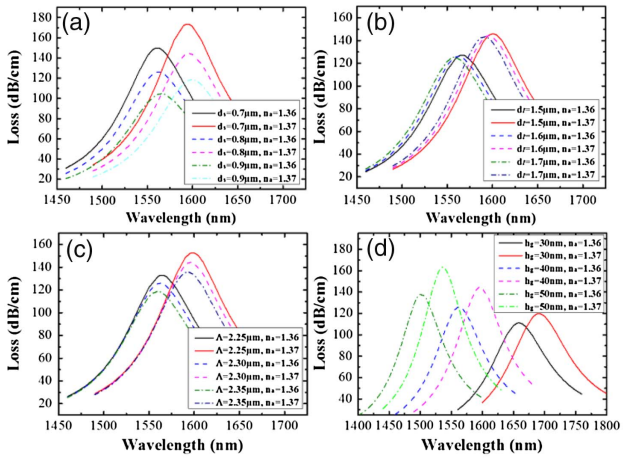

Fig. 3. Variation of confinement loss as a function of wavelength with varying (a) diameter of small air holes d_s, (b) diameter of large air hole d_l, (c) lattice pitch of air holes Λ, and (d) gold grating thickness h_g, when the RI changes from 1.36 to 1.37.

Table 1, different diameters of small air hole have little influence on the wavelength sensitivity. Moreover, we also investigated the sensitivity variation, when the diameter of large air holes (d_l) changes. Figure 3(b) illustrates the loss spectra of a gold grating SPR sensor with different diameters of large air holes. With increasing of the diameter, the loss slightly deduces, and the resonance wavelength shifts to shorter wavelength. But the diameter of large air holes has limited influence on the wavelength sensitivity, as shown in Table 2. The lattice pitch (Λ) also was investigated, and the loss spectra are shown in Fig. 3(c). With increasing of the pitch, the resonance wavelength shows slightly blueshift and confinement loss decreases. The reason is that large pitch results in changing of the phase-matching condition. As shown in Table 3, a different lattice pitch has a slight influence on wavelength sensitivity. Parameters of gold grating also play a vital role in performance of PCF-SPR sensors. As shown in Fig. 3(d), with increasing of the gold grating thickness, more energy of the core mode is used for overcoming the damping loss, and the resonance wavelength shifts toward a shorter wavelength. When the thickness of gold grating increases, the sensitivity slightly increases, as shown in Table 4. To optimize the performance of the gold grating SPR sensor, the resonance wavelength is selected around 1550 nm, and the structure parameters of PCF this should be $d_s = 0.8$ μm, $d_l = 1.6$ μm, and $\Lambda = 2.3$ μm, and the thickness of gold should be $h_g = 40$ nm.

The gold grating parameters were also investigated for improving the performance of the SPR sensor. As shown in Fig. 4(a), a different grating constant (d_0) results in a different resonance wavelength, and the wavelength sensitivity also changes, as shown in Table 5. We can also observe that, with

Table 1. Relationship Between d_s and Wavelength Sensitivity (S_w)

d_s (μm)	0.7	0.8	0.9
S_w (nm/RIU)	3320	3354	3390

Table 2. Relationship Between d_l and Wavelength Sensitivity (S_w)

d_l (μm)	1.5	1.6	1.7
S_w (nm/RIU)	3382	3354	3328

Table 3. Relationship Between Λ and Wavelength Sensitivity (S_w)

Λ (μm)	2.25	2.3	2.35
S_w (nm/RIU)	3368	3354	3344

Table 4. Relationship Between h_g and Wavelength Sensitivity (S_w)

h_g (nm)	30	40	50
S_w (nm/RIU)	3244	3354	3412

increasing of the grating constant, the loss increases, which results in higher amplitude sensitivity. Therefore, the grating constant can be used to modulate the resonance wavelength. It is possible for SPR sensors working in expected wavelengths such as in a common commercial broadband laser. Figure 4(b) depicts the loss spectra of gold grating with different duty ratio (η). We can see that, with increasing of duty ratio, the confinement loss increases significantly. When the duty ratio increases, the FWHM reduces, which can obtain a better signal-to-noise (SNR) ratio. However, the sensitivity slightly decreases, as

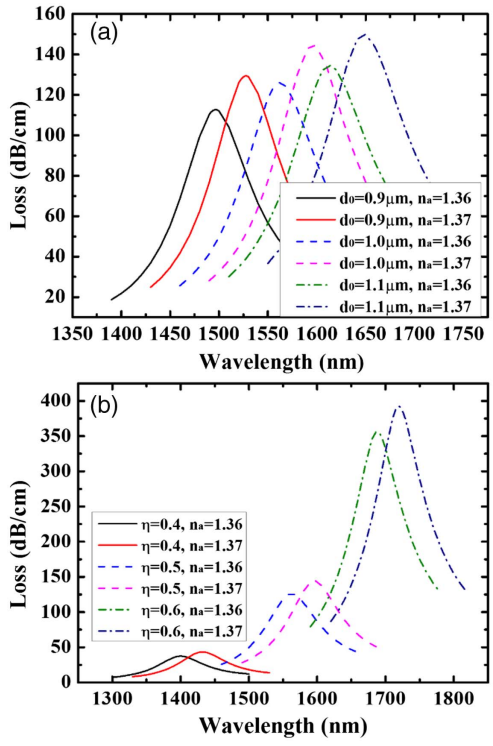

Fig. 4. Variation of confinement loss with varying (a) grating constant d_0 and (b) duty ratio η, when the RI changes from 1.36 to 1.37.

Table 5. Relationship Between d_0 and Wavelength Sensitivity (S_w)

d_0 (μm)	0.9	1.0	1.1
S_w (nm/RIU)	3108	3354	3564

Table 6. Relationship Between η and Wavelength Sensitivity (S_w)

η	0.4	0.5	0.6
S_w (nm/RIU)	3196	3354	3176

shown in Table 6. Thus, the grating constant is set as $d_0 = 1$ μm, and the duty ratio could be set as $\eta = 0.5$.

Because the SPR sensor is extremely sensitive to the change of surrounding environment RI, we investigated the transmission spectra by changing the analyte RI. From Fig. 5(a), we can see that, with increasing of the RI, the resonance wavelengths are redshifted. Therefore, the analyte RI could be detected by measuring the shift of resonance wavelength. As shown in Fig. 5(b), with increasing of analyte RI, the resonance wavelength shows good linear response, and the wavelength sensitivity reaches to 3340 nm/RIU. In addition, with increasing of analyte RI, the effective index of SPP mode is close to that of the core mode, which results in more energy loss of the core mode. Therefore, the amplitude also can be used to sensing the RI as a convenient and cost-effective method. The amplitude sensitivity can be defined from [15]

$$s_A(\mathrm{RIU}^{-1}) = -\frac{1}{\alpha(\lambda, n_a)}\frac{\partial\alpha(\lambda, n_a)}{\partial n_a}, \tag{4}$$

where $\alpha(\lambda, n_a)$ is the loss at RI of n_a, and $\partial\alpha(\lambda, n_a)$ is the loss difference between two adjacent analyte RIs.

Figure 5(c) shows the amplitude sensitivity of the proposed SPR sensor calculated by Eq. (4). From Fig. 5(c), maximum amplitude sensitivity can be obtained at the wavelength of

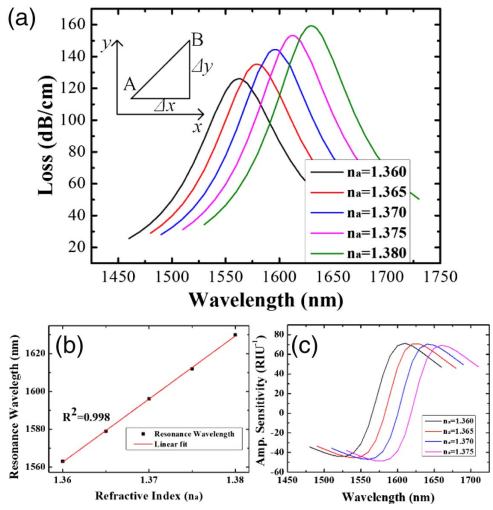

Fig. 5. (a) Variation of confinement loss as a function of wavelength with different analyte RI. (b) Wavelength sensitivity with the analyte RI range from 1.36 to 1.38. (c) Amplitude sensitivity with the variation of analyte RI.

1660 nm, which is −69.3 RIU^{-1}. Based on the theory mentioned in [6], the two-feature (2F) sensitivity combines wavelength sensitivity and amplitude sensitivity for enhancing the RI sensitivity. As shown in the embedded image in Fig. 5(a), if we detect the RI difference Δn of analyte and resonance wavelength shifts from A to B, the 2F sensitivity can be defined as

$$S_{2\mathrm{F}} = \frac{\overline{AB}}{\Delta n} = \frac{\sqrt{\Delta x^2 + \Delta y^2}}{\Delta n}. \tag{5}$$

By normalizing Δx and Δy, we can make wavelength sensitivity and amplitude sensitivity into one dimension. For example, when analyte RI changes from 1.37 to 1.375, wavelength shifts from 1596.10 to 1612.44 nm and loss shifts from 144.42 to 153.24 dB/cm, which means $\Delta x = 16.34$ nm, $\Delta y = 8.82$ dB/cm and $\Delta n = 0.005$, respectively. We assume the length of sensing area is 1 cm. If the wavelength resolution is 0.02 nm (AQ3617B) and amplitude resolution is 0.05 dB, the RI change will bring 817 data intervals for the x axis ($DI_x = 16.34/0.02 = 817$) and 176 data intervals for the y axis ($DI_y = 8.82/0.05 = 176$). Therefore, the 2F data intervals $DI_{2\mathrm{F}} = (817^2 + 176^2)^{1/2} = 836$. Finally, the maximum theoretical resolution of wavelength (R_w), amplitude (R_a), and $R_{2\mathrm{F}}$ can be calculated by

$$R = \frac{\Delta n}{DI} = \frac{\Delta n}{\sqrt{DI_x^2 + DI_y^2}}. \tag{6}$$

Results show that 2F resolution ($R_{2\mathrm{F}} = 5.98 \times 10^{-6}$ RIU) is higher than theoretical wavelength resolution ($R_w = 6.12 \times 10^{-6}$ RIU) and theoretical amplitude resolution ($R_a = 2.84 \times 10^{-5}$ RIU).

4. CONCLUSION

A practical D-shaped photonic crystal fiber RI sensor based on surface plasmon resonance is demonstrated by putting a gold grating on a flat plane. FEM has been used to analyte the performance of this proposed SPR sensor. The simulation results show that PCF structure parameters have little influence on the sensor performance. The gold grating is used to enhance the sensitivity and tune the resonance wavelength. Using the 2F interrogation method, the maximum theoretical resolution of RI is improved significantly and reaches to 5.98×10^{-6} RIU, which is much higher than wavelength and amplitude resolution. By taking advantage of the latest nanofabrication technique, the proposed structure can be utilized for environmental, biological, and biochemical sensing applications.

Funding. National Key Research and Development Program of China (2017YFF02098-01); Natural Science Foundation of Guangxi Province (ZR201709200426); Natural Science Foundation of Shandong Province (ZR2018MF031); National Natural Science Foundation of China (NSFC) (11504070).

REFERENCES

1. P. Singh, "SPR biosensors: historical perspectives and current challenges," Sens. Actuators B **229**, 110–130 (2016).

2. A. A. Rifat, G. A. Mahdiraji, Y. M. Sua, Y. G. Shee, R. Ahmed, D. M. Chow, and F. R. M. Adikan, "Surface plasmon resonance photonic crystal fiber biosensor: a practical sensing approach," IEEE Photon. Technol. Lett. **27**, 1628–1631 (2015).
3. R. C. Jorgenson and S. S. Yee, "A fiber-optic chemical sensor based on surface plasmon resonance," Sens. Actuators B **12**, 213–220 (1993).
4. F. Wang, Z. Sun, C. Liu, T. Sun, and P. K. Chu, "A highly sensitive dual-core photonic crystal fiber based on a surface plasmon resonance biosensor with silver-graphene layer," Plasmonics **12**, 1–7 (2016).
5. R. K. Gangwar and V. K. Singh, "Highly sensitive surface plasmon resonance based D-shaped photonic crystal fiber refractive index sensor," Plasmonics **12**, 1367–1372 (2016).
6. Y. Chen, Q. Xie, X. Li, H. Zhou, X. Hong, and Y. Geng, "Experimental realization of D-shaped photonic crystal fiber SPR sensor," J. Phys. D **50**, 025101 (2017).
7. J. N. Dash and R. Jha, "Graphene-based birefringent photonic crystal fiber sensor using surface plasmon resonance," IEEE Photon. Technol. Lett. **26**, 1092–1095 (2014).
8. B. Shuai, L. Xia, Y. Zhang, and D. Liu, "A multi-core holey fiber based plasmonic sensor with large detection range and high linearity," Opt. Express **20**, 5974–5986 (2012).
9. A. A. Rifat, F. Haider, R. Ahmed, G. A. Mahdiraji, F. R. M. Adikan, and A. E. Miroshnichenko, "Highly sensitive selectively coated photonic crystal fiber-based plasmonic sensor," Opt. Lett. **43**, 891–894 (2018).
10. A. Hassani and M. Skorobogatiy, "Design of the microstructured optical fiber-based surface plasmon resonance sensors with enhanced microfluidics," Opt. Express **14**, 11616–11621 (2006).
11. Z. Fan, S. Li, Q. Liu, G. An, H. Chen, J. Li, D. Chao, H. Li, J. Zi, and W. Tian, "High sensitivity of refractive index sensor based on analyte filled photonic crystal fiber with surface plasmon resonance," IEEE Photon. J. **7**, 4800809 (2015).
12. E. K. Akowuah, T. Gorman, H. Ademgil, S. Haxha, G. K. Robinson, and J. V. Oliver, "Numerical analysis of a photonic crystal fiber for biosensing applications," IEEE J. Quantum Electron. **48**, 1403–1410 (2012).
13. P. B. Johnson and R. W. Christy, "Optical constants of the noble metals," Phys. Rev. B **6**, 4370–4379 (1972).
14. F. Chiavaioli, C. A. J. Gouveia, P. A. S. Jorge, and F. Baldini, "Towards a uniform metrological assessment of grating-based optical fiber sensors: from refractometers to biosensors," Biosensors **7**, 23 (2017).
15. M. R. Hasan, S. Akter, A. A. Rifat, S. Rana, K. Ahmed, R. Ahmed, H. Subbaraman, and D. Abbott, "Spiral photonic crystal fiber-based dual-polarized surface plasmon resonance biosensor," IEEE Sens. J. **18**, 133–140 (2018).